Optical Materials 50 (2015) 268–274

Contents lists available at ScienceDirect

Optical Materials

journal homepage: www.elsevier.com/locate/optmat

Energy transfer and energy level decay processes of Er^{3+} in water-free tellurite glass

Laercio Gomes [a], Daniel Rhonehouse [b], Dan T. Nguyen [b], Jie Zong [b], Arturo Chavez-Pirson [b], Stuart D. Jackson [c,*]

[a] Center for Lasers and Applications, IPEN/CNEN-SP, P.O. Box 11049, São Paulo, SP 05422-970, Brazil
[b] NP Photonics, 9030 S. Rita Road, Tucson, AZ 85747, USA
[c] MQ Photonics, Department of Engineering, Faculty of Science and Engineering, Macquarie University, North Ryde 2109, Australia

ARTICLE INFO

Article history:
Received 15 October 2015
Received in revised form 5 November 2015
Accepted 5 November 2015
Available online 11 November 2015

Keywords:
Mid-infrared spectroscopy
Fiber laser
Time resolved spectroscopy
Optical fiber technology

ABSTRACT

This report details the fundamental spectroscopic properties of a new class of water-free tellurite glasses studied for future applications in mid-infrared light generation. The fundamental excited state decay processes relating to the $^4I_{11/2} \rightarrow {}^4I_{13/2}$ transition in singly Er^{3+}-doped Tellurium Zinc Lanthanum glass have been investigated using time-resolved fluorescence spectroscopy. The excited state dynamics was analyzed for Er_2O_3 concentrations between 0.5 mol% and 4 mol%. Selective laser excitation of the $^4I_{11/2}$ energy level at 972 nm and selective laser excitation of the $^4I_{13/2}$ energy level at 1485 nm has established that in a similar way to other Er^{3+}-doped glasses, a strong energy-transfer upconversion by way of a dipole–dipole interaction between two excited erbium ions in the $^4I_{13/2}$ level populates the $^4I_{11/2}$ upper laser level of the 3 μm transition. The $^4I_{13/2}$ and $^4I_{11/2}$ energy levels emitted luminescence with peaks located at 1532 nm and 2734 nm respectively with luminescence efficiencies of 100% and 8% for the higher (4 mol.%) concentration sample. Results from numerical simulations showed that a population inversion is reached at a threshold pumping intensity of ~57 kW cm^{-2} for a CW laser pump at 976 nm for $[Er_2O_3]$ = 2 mol.%.

1. Introduction

There is growing interest in developing high power and efficient sources of midinfrared light for applications in defence, industry, medicine and sensing. Sources developed using the optical fiber as the gain medium have seen rapid development with high power [1] and ultrashort pulse emission [2,3] recently demonstrated. All demonstrations setting power and efficiency records have involved fluoride glass as the host medium because this material is by far the most developed and is available from a number of commercial suppliers. Whilst there is a strong need to continue the research using this material for better power and efficiency, the measured degradation [4] of the performance of the laser as a result of atmospheric OH incorporation into the end facets of the fiber, a process that scales quickly with emitted power from the fiber laser, has forced engineered solutions, e.g., end capping the fiber ends to improve reliability. Whilst this technique does allow good and reliable emission up to the 10s of Watt level, it is still an open question as to whether this approach will lead to much higher power emission to the 100s of Watt level.

The heavy metal oxide glasses, in particular the tellurites, are a large family of glasses that exhibit good infrared transmission and have been researched for some time. Unfortunately, to date they have not produced emission beyond approximately 2 μm [5]. This is a disappointing situation because heavy metal oxide glasses have the potential to be a robust alternative to the fluoride glass family. Tellurite glasses have relatively low maximum phonon energies (~690 cm^{-1} for the Tellurium Zinc Lanthanum glass composition used here) when compared to other oxide glasses. In addition, they have good transmission between 0.35 and 5 μm and are less susceptible to the crystallization and degradation that can occur in the fluoride glass compositions. There are a number of reasons for the poor performance of these glasses relative to the fluoride glasses. Firstly for most compositions, the maximum phonon energy is still too large which leads to low luminescence efficiencies for the $^4I_{11/2} \rightarrow {}^4I_{13/2}$ transition, the shortest and most widely studied of the mid-infrared emission wavelengths. Secondly, water contamination either from the precursor materials or during the fabrication of the glass or fiber lead not only to an increase in light absorption at the short (3 μm) region of the mid-infrared, but

* Corresponding author.
E-mail address: stuart.jackson@mq.edu.au (S.D. Jackson).

http://dx.doi.org/10.1016/j.optmat.2015.11.007
0925-3467/

fluorescence transitions that are resonant with the vibrational mode of the OH radical are heavily quenched [6] by way of energy transfer to the OH radical which further impacts performance. Thus, in parallel with the development of alternative tellurite glasses that have lower maximum phonon energies, development of glasses that are essentially "water-free" would provide a boost to the applications potential for this important class of rare earth host material. In recent work, we have successfully produced a tellurite glass that is essentially water-free [7]. Low loss optical fibers based on this glass have been fabricated for a range of light transport applications in the mid-infrared and undoped single mode fibers have been used to generate a broadband supercontinuum with wavelength coverage that extends from 1 μm to 5 μm [8]. Rare earth doping of this fiber is expected to be valuable as a gain medium for high power fiber lasers operating in the midinfrared.

To explore the light emission potential of the $^4I_{11/2} \rightarrow {}^4I_{15/2}$ transition in tellurite glass and more broadly to investigate the possibility of an efficient laser operating at 3 μm in an oxide-based glass, detailed spectroscopic studies are required. In this report, we investigate the luminescence properties of Er^{3+}-doped tellurite glass that have very low levels of water contamination. We carry out the basic spectroscopic measurements, compare the results with other previously reported tellurite glasses and asses their suitability for emission in the mid-infrared. We have prepared a number of Er_2O_3-doped tellurite glasses of varying Er_2O_3 concentration (from 0.5 to 4 mol.%) and measured the luminescence decay characteristics after selective energy level excitation. The luminescence efficiency of these levels was determined when the experimental decay time was compared with the radiative lifetimes calculated using Judd–Ofelt theory. Due to the high O-H phonon energy, the cross-relaxation and energy transfer to OH^- impurities in the host glass results in the depopulation of the $^4I_{11/2}$ and $^4I_{13/2}$ energy levels and the rapid decay of the excited ions back to the ground state. The energy transfer rates to the OH^- groups in the glass were measured for these energy levels. Measurements of the pump excited state absorption (ESA), energy transfer upconversion (ETU) and cross-relaxation (CR) parameters have been obtained.

2. Experimental procedure

The Er^{3+}-doped tellurite glass samples were prepared from high purity raw materials with 99.999% pure TeO_2, ZnF, ZnO_2, and La_2O_3. The starting powder materials were melted in a Au crucible in a dry glovebox environment, reducing the OH content in the glass, at 875 °C for 6 h. The liquids were poured into polished aluminum molds and annealed at 360 °C for 18 h to remove any mechanical stresses. The samples were cut and polished into $10 \times 10 \times 12$ mm^3 rectangular prisms. The Er^{3+} ion densities in the samples were calculated to be 2.3×10^{20} cm^{-3}, 4.6×10^{20} cm^{-3}, 9.2×10^{20} cm^{-3} and 1.84×10^{21} cm^{-3} for the doped tellurite samples with 0.5, 1, 2 and 4 mol.% Er_2O_3, respectively.

This composition has the advantage of its maximum phonon energy being determined by tellurium oxide itself versus other well known tellurium glasses containing additional components such as W, Al, Nb, Ge as stabilizers. All other glass constituents present in TZL (Zn, La) have lower phonon energies than tellurium. Additionally the highest phonon energy components consist of distorted TeO_4 pyramids or so-called TeO(3 + 1) species (with phonon energy of ~690 cm^{-1}) which make up only a minority of the Te species present in the glass structure. This leads to lower maximum phonon densities and lower phonon rates as the majority of vibrational species have phonon energies < 650 cm^{-1}.

The absorption spectra in the range of 2000–10,000 nm were measured using a FTIR spectrophotometer (Nicolet 6700). The decay characteristics of the excited states of Er^{3+} were measured using pulsed 13 mJ (4 ns, 10 Hz) laser excitation from a tunable optical parametric oscillator (OPO) pumped by the second harmonic of a *Q*-switched Nd-YAG laser (Brilliant B from Quantel). Tunable laser excitation from the OPO was used to directly excite the $^4I_{11/2}$ energy level at 972 nm and $^4I_{13/2}$ energy level at 1485 nm. The infrared luminescence (for $\lambda > 1080$ nm) was detected using an InSb infrared detector (Judson model J-10 D cooled to 77 K) in conjunction with a fast preamplifier with a response time of ~0.5 μs and analyzed using a digital 200 MHz oscilloscope (Tektronix TDS 410). The visible and near infrared ($\lambda < 1100$ nm) was detected using a photomultiplier tube (EMI) with a sensitive cathode of S-1 type (PMT EMI refrigerated at −20 °C) with a response time of 20 ns. All the fluorescence decay characteristics were measured at 300 K. To isolate the infrared luminescence signals, bandpass filters each with ~80% transmission at 1500 nm or 2750 nm with a half width of 25 nm and an extinction coefficient of $\sim 10^{-5}$ outside this band were used.

3. Experimental results

As with most other Er^{3+}-doped glasses, when Er^{3+}-doped tellurite glass is excited at 972 nm the main processes involving the energy levels are: (*a*) Ground state absorption (GSA), Er^{3+} ($^4I_{15/2}$) + hν (972 nm) → Er^{3+} ($^4I_{11/2}$), (*a*′) Excited state absorption (ESA), Er^{3+} ($^4I_{11/2}$) + hν (972 nm) → Er^{3+} ($^4F_{7/2}$) + $\hbar\omega$ → Er^{3+} ($^4S_{3/2}$), (*b*) Energy transfer upconversion (ETU), Er^{3+} ($^4I_{13/2}$) + Er^{3+} ($^4I_{13/2}$) → Er^{3+} ($^4I_{9/2}$), (There should be other transfer energy upconversion processes in this system of Er^{3+}-ions for simplicity, however, we can ignore those terms as their magnitudes would be small as compared with above terms.) (*c*) Cross-relaxation (CR), Er^{3+} ($^4S_{3/2}$) + Er^{3+} ($^4I_{15/2}$) → Er^{3+} ($^4I_{9/2}$) + Er^{3+}($^4I_{13/2}$).

3.1. Infrared absorption spectra

Fig. 1 shows the infrared absorption spectra of the Er_2O_3 (1 and 2 mol.%)-doped tellurite glass used in this work. The spectrum shows a broad, strong absorption band between 2500 and 3500 cm^{-1}, which is attributed to free OH^- groups in oxide glass [9]. The absorption coefficient (of the OH^- vibration band at 3053 cm^{-1} due to the free OH^- group is given by $N_{OH} = \frac{N_{Av}\alpha}{\xi}$, where N_{Av} is the Avogadro constant (6.02×10^{23}), α is the absorption coefficient (cm^{-1}) and ξ is the absorptivity of free OH^- groups in the glass. Using $\xi = 49.1 \times 10^3$ cm^2 mol^{-1} [10] we estimate the OH^- concentration in our samples as $N_{OH} = 2.42 \times 10^{17}$ cm^{-3} (for $[Er^{3+}] = 2.3 \times 10^{20}$ cm^{-3}) with $\alpha = 0.0197$ cm^{-1}; $N_{OH} = 6.50 \times 10^{16}$ OH^- cm^{-3} (for $[Er^{3+}] = 4.6 \times 10^{20}$ cm^{-3}) with $\alpha = 0.0053$ cm^{-1}; $N_{OH} = 2.59 \times 10^{17}$ cm^{-3} (for $[Er^{3+}] = 9.6 \times 10^{20}$ cm^{-3}) with $\alpha = 0.021$ cm^{-1} and $N_{OH} = < 2.4 \times 10^{17}$ cm^{-3} (for $[Er^{3+}] = 1.84 \times 10^{21}$ cm^{-3}) and $\alpha < 0.002$ cm^{-1}. The highest absorption coefficient corresponding to the $[Er^{3+}] = 9.2 \times 10^{20}$ cm^{-3} sample, of 0.021 cm^{-1}, is fifty times smaller than that measured previously in tellurite glasses melted in a dry atmosphere [11]. The concentrations of OH^- in the glass samples that were studies are given in Table 1.

3.2. Luminescence decay of $^4I_{11/2}$ level

When the samples were excited at 972 nm, the typical green luminescence from $^4S_{3/2}$ excited state of Er^{3+} was observed. A best fit to the $^4I_{11/2}$ decay was determined using the Burshtein function [12], which has γ and t_1 as parameters.

$$I(t) = I_0 \exp\left(-\gamma\sqrt{t} - \frac{t}{t_1}\right), \quad (1)$$

where γ is used as a curve fitting to cater for the non-exponential component of the luminescence decay and $t_1 = \frac{\tau_d}{1+\omega\tau_d}$ is the exponential decay component that accounts for the intrinsic decay rate

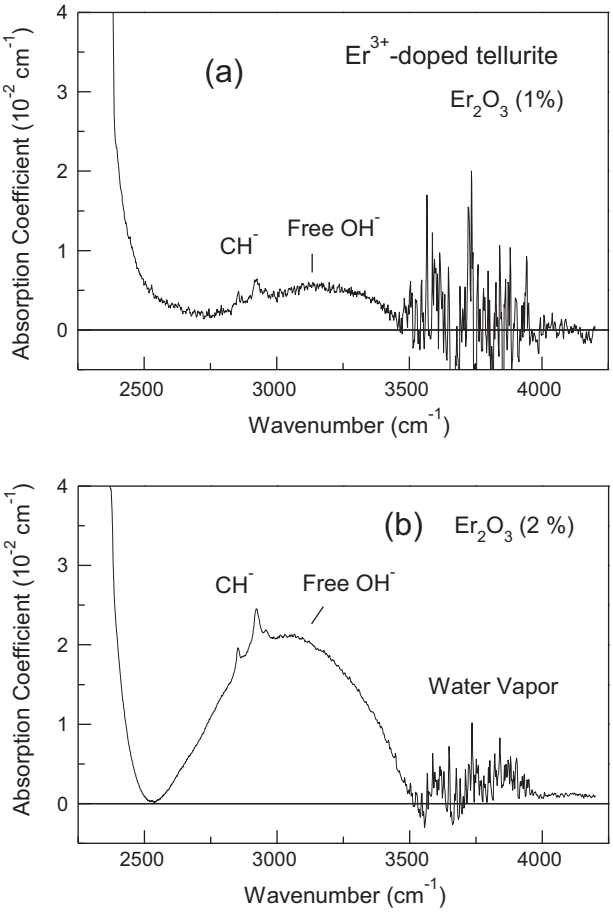

Fig. 1. Measured absorption spectrum of Er_2O_3 (1 and 2 mol.%)-doped tellurite showing the free OH^- group absorption band near 3053 cm^{-1}.

Table 1
Measurements of OH in Er^{3+}-doped (water-free) tellurite glass.

Sample (Er_2O_3)	O.D.	α (cm^{-1})	N_{OH} (cm^{-3})
0.5%	0.01028	0.01973	2.42×10^{17}
1%	0.00228	0.00530	6.50×10^{16}
2%	0.01099	0.02109	2.59×10^{17}
4%	<0.0010	<0.0019	$<2.4 \times 10^{16}$

(radiative + non-radiative multiphonon decay) of the donnor state, τ_d, and the migration assisted donor to acceptor energy-transfer rate, ω. The mean lifetime is obtained by the integration of the decay curve using Eq. (2). This contains both the exponential and non-radiative components of the fluorescence decay into the one parameter (τ).

$$\tau = \int_0^\infty \exp\left(-\gamma\sqrt{t} - \frac{t}{t_1}\right)dt. \quad (2)$$

The best fitting parameters and the integrated lifetime are given in Table 2. The experimental decay curves are shown in the Fig. 2.

3.3. Luminescence decay of the $^4I_{13/2}$ level

Laser excitation at 1500 nm with an average energy of 7 mJ per pulse and 4 ns duration was used for this part of the experiment. A weak green luminescence from the $^4S_{3/2}$ excited level was observed due to the ESA and ETU. A best fit to the luminescence decay of the $^4I_{13/2}$ state was accomplished using the Burshtein function, Eq. (1), the parameters providing the best fit and the resulting integrated

Table 2
Best fitting parameters obtained for the luminescence decay of $^4I_{11/2}$ excited level of Er^{3+} in (water-free) Er^{3+}-doped tellurite glasses.

[Er_2O_3] (mol.%)	γ ($s^{-1/2}$)	t_1 (μs)[a]	R^2	τ (μs) (integrated)
0.5	12.7	326	0.9998	267
1	9.8	279	0.9999	242
2	6.9	253	0.9999	230
4	14.5	251	0.9990	206

[a] Intrinsic lifetime of $^4I_{11/2}$ level is equal to 314 μs.

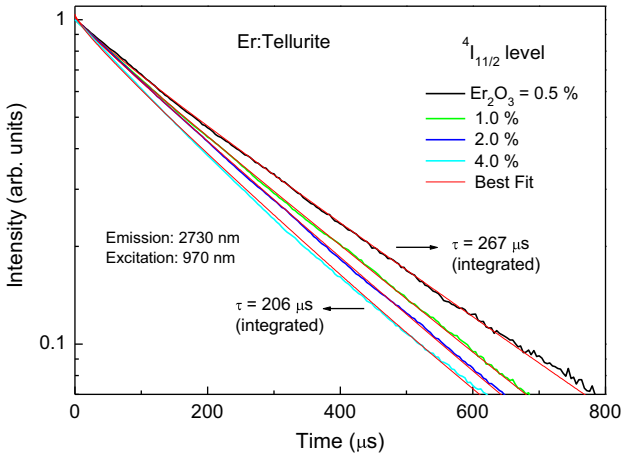

Fig. 2. Emission decay curves measured at 2730 nm using a laser excitation at 970 nm. Er^{3+}-doped tellurite glasses with Er_2O_3 equal to 0.5, 1, 2 and 4 mol.% were used.

lifetime are giving in Table 3. The experimental decay curves are shown in the Fig. 3.

3.4. Energy transfer upconversion from the $^4I_{11/2}$ excited level

An analysis of the ETU process was carried out using the 2730 nm emission from the $^4I_{11/2}$ level produced by excitation of the $^4I_{15/2}$ energy level at 1485 nm (average energy of 13 mJ per pulse and pulse duration of 4 ns). Fig. 4 shows the luminescence time transient measured for [Er_2O_3] = 2 mol.% for many excitation densities. In this figure one can observe that for a low excitation density of 1.5×10^{18} cm^{-3}, only ESA processes are observed, however, the contribution from ESA decreases and the ETU process begins to dominate the decay of the 2730 nm emission as the excitation density increases to 1.5×10^{19} cm^{-3}.

Fig. 5 shows the luminescence upconversion transient measured at 2730 nm after laser excitation at 1485 nm for Er^{3+}-doped tellurite glass with [Er_2O_3] = 2 mol.%. The curve of best fit was obtained using Eq. (3).

$$I(t) = A\exp(-t/\tau_1) + B[\exp(-\gamma_2\sqrt{t} - t/\tau_2) - \exp(-t/\tau_{rise})], \quad (3)$$

where A is the amplitude of the ESA process and B is the amplitude of the ETU process. τ_1 is the intrinsic decay time constant of $^4I_{11/2}$

Table 3
Parameters providing the best fit obtained for the luminescence decay of $^4I_{13/2}$ excited level of Er^{3+} in Er_2O_3-doped tellurite glass.

[Er_2O_3] (mol.%)	γ ($s^{-1/2}$)	t_1 (ms)[a]	R^2	τ (ms) (integrated)
0.5	2.9	6.5	0.997	5.3
1	2.3	7.7	0.998	6.5
2	2.2	8.7	0.999	7.3
4	2.5	10.3	0.999	8.3

[a] Intrinsic lifetime of $^4I_{13/2}$ level is equal to 3.27 ms.

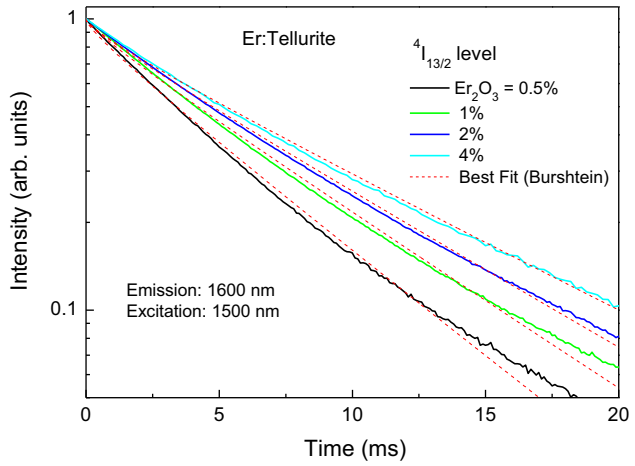

Fig. 3. Luminescence decay curves measured at 1600 nm after a pulse laser excitation at 1500 nm. Er^{3+}-doped tellurite glasses with Er_2O_3 equal to 0.5, 1, 2 and 4 mol.% were used. An increasing $^4I_{13/2}$ level lifetime is observed due to excitation migration of the $^4I_{13/2}$ levels with the increasing Er^{3+} concentration.

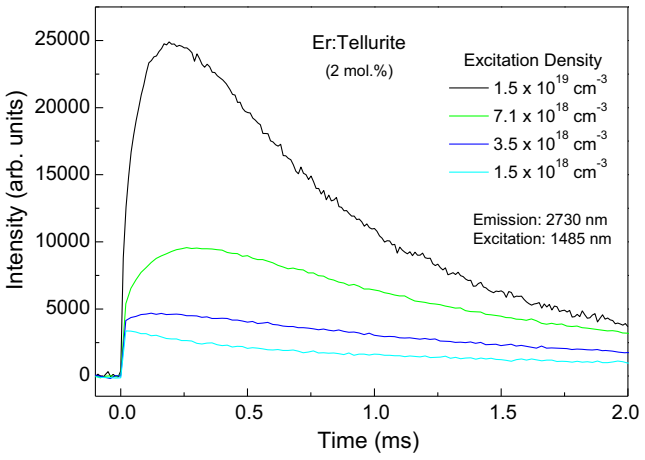

Fig. 4. Upconversion luminescence transient measured at 2730 nm for Er:tellurite glass with Er_2O_3 = 2 mol.% under laser pulse excitation at 1485 nm. ETU gradually dominates the emission properties of the 2730 nm emission as the excitation increases.

level (314 μs) for Er^{3+}-doped tellurite and γ_2 and τ_2 are the parameters of the ETU process that is strongly affected by the excitation migration through the $^4I_{13/2}$ level, which increases the donnor lifetime from 3.27 ms (intrinsic lifetime) to 8.3 ms for Er_2O_3 = 4 mol.%. This strong excitation migration verified for the $^4I_{13/2}$ level (factor of 2.54) should extend the ETU time-span and therefore increasing the decay time of the $^4I_{11/2}$ as observed in Fig. 4. Neverthless, the most important information about the ETU time process is given by the rise time (τ_{rise}) of the luminescence transient observed in Fig. 4 (and given by Eq. (3)) that is dependent on the excitation intensity and is not affected by the increasing donor lifetime. The relative contribution from ETU was determined using $f_{ETU} = B/(A + B)$ and the relative ESA contribution is given by $f_{ESA} = A/(A + B)$.

The rate probability (s^{-1}) for ETU was obtained using the relation $W_{ETU} = \frac{1}{\tau_{rise}} - \frac{1}{\tau_D}$, where τ_D is the intrinsic lifetime of $^4I_{13/2}$ level, i.e., 3.27 ms. Fig. 6 shows the W_{ETU} rates as a function of the excitation density of the Er^{3+} ions for Er_2O_3 = 2 mol.% after laser excitation at 1485 nm for several excitation intensities. In this figure one can observe that the rate of ETU tends to a value $K_0 = 9100\ s^{-1}$ according to the critical radius model used to fit the experimental data. The critical radius model has been applied with success to

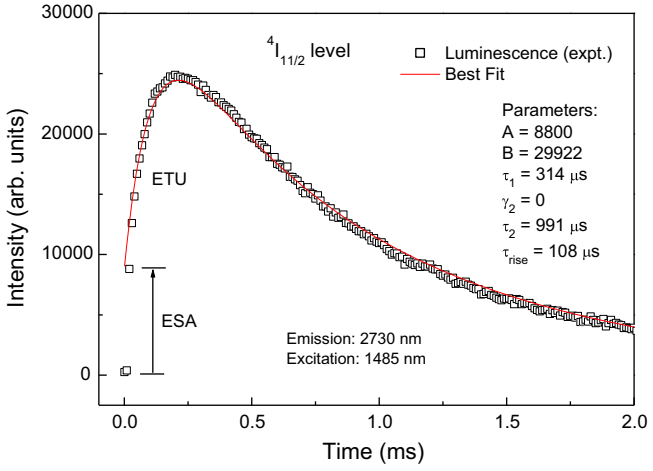

Fig. 5. Measured luminescence transient from $^4I_{11/2}$ level at 2730 nm (squares) after laser excitation at 1485 nm (E = 13 mJ) at T = 300 K for Er^{3+}-doped tellurite glass with Er_2O_3 = 2 mol.% (or $Er^{3+} = 9.2 \times 10^{20}$ cm^{-3}) and an excitation density of $\sim 1.4 \times 10^{19}$ Er^{3+} cm^{-3}. The best fit to the 2730 luminescence (red solid line) was obtained using Eq. (3) (R^2 = 0.989). f_{ESA} is equal to 0.23 and f_{ETU} = 0.77 (or 77% contribution). (For interpretation of the references to color in this figure legend, the reader is referred to the web version of this article.)

describe the ETU rate probability (s^{-1}) due to the two interacting $^4I_{13/2}$ excited states of Er^{3+} in laser materials as the excitation density increases in laser crystals and glasses [6,13].

A similar procedure was carried out to find the rate constant probability K_0 for other Er_2O_3 concentrations (i.e., 0.5, 1 and 4 mol.%), Fig. 7 shows the ETU rate constant K_0 (s^{-1}) as a function of Er_2O_3 concentration. Fig. 7 shows that the ETU rate constant K_0 (s^{-1}) increases with the Er^{3+} concentration increasing and tends to a constant value for $Er^{3+} \sim 2.5 \times 10^{21}$ cm^{-3}. This behaviour suggests the existance of a critical concentration (N_C) of Er^{3+} for the Er^{3+} ($^4I_{11/2}$) × Er^{3+} ($^4I_{11/2}$) energy-transfer upconversion process (ETU) where the K_0 (s^{-1}) rate tends to a constant value for [Er^{3+}] > N_C (see the experimental data represented by squares in Fig. 7). A best fit to the rate constant probability of ETU was carried using Eq. (4); the ETU efficiency will increase if an Er^{3+} ion excited to the $^4I_{13/2}$ level transfers its energy to another excited Er^{3+} ($^4I_{13/2}$) ion within the a critical distance, R_C, with an ETU augmentation efficiency, η_{ETU}, dependent on [Er^{3+}]. This model predicts a saturation

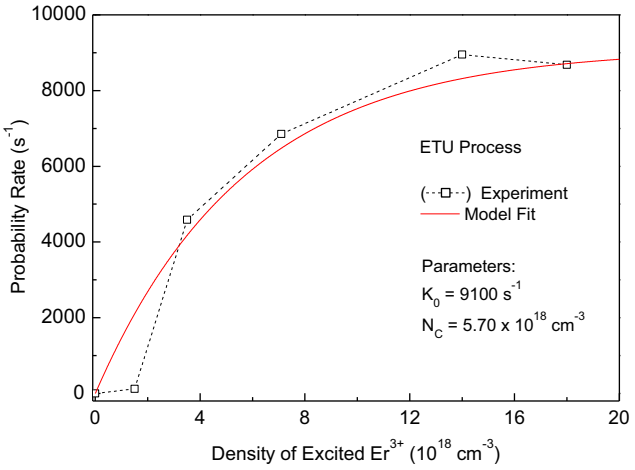

Fig. 6. Measured ETU rate probability (s^{-1}) as a function of the excited Er^{3+} ion density (N^*) obtained by measuring the luminescence transient of the $^4I_{11/2}$ level (2730 nm) after pulsed (4 ns) excitation at 1485 nm (squares). The solid line represents the best fit using the critical radius model. [Er_2O_3] = 2 mol.%.

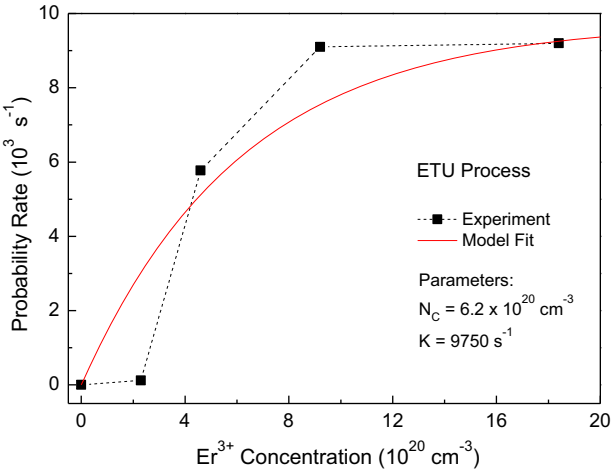

Fig. 7. Measured ETU rate constant K_0 (s^{-1}) as a function of the Er^{3+} concentration (ions cm^{-3}). The solid line represents the best fit using the critical radius model given by Eq. (4).

of the ETU rate (K_0) to a constant value K_S, which is reached for $N_{Er} > N_C$, where N_C is the critical concentration. The ETU rate constant augmentation efficiency is given by

$$K_0 = \eta_{ETU} K_S \quad \text{and} \quad \eta_{ETU} = 1 - \exp\left(-\frac{N_{Er}}{N_C}\right) \tag{4}$$

where η_{ETU} is the ETU efficiency, K_0 is the rate constant parameter of ETU process and N_{Er} is the Er^{3+} concentration. N_C is the critical concentration of Er^{3+}, which is equal to 6.2×10^{20} cm^{-3} and $K_S = 9750$ s^{-1} for ETU process in Er_2O_3-doped tellurite glass. Table 4 shows all the energy transfer rate parameters determined in this work.

4. Rate equation modeling

Fig. 8 shows the simplified energy level scheme of the Er^{3+}-doped tellurite system considered for CW diode laser pumping at 976 nm. n_1, n_2, n_3, n_4 and n_5 are the populations in the $^4I_{15/2}$, $^4I_{13/2}$, $^4I_{11/2}$, $^4F_{9/2}$ and $^4S_{3/2}$ energy levels of Er^{3+}, the most important and relevant energy levels participating in the laser transition of Er^{3+} at 2.75 μm. The $^4F_{7/2}$ and $^2H_{11/2}$ excited levels were not considered because they are strongly depopulated by fast multiphonon decay to the $^4S_{3/2}$ level, the next lower long-lived state. (This is also the case for $^4I_{9/2}$ level that non-radiatively decays to the $^3I_{11/2}$ state.)

The rate equations for the simplified system for 976 nm pumping comprising the model and using the fact that $n_1 + n_2 + n_3 + n_4 + n_5 = 1$ (normalized population of Er^{3+}) are

$$\frac{dn_1}{dt} = -R_P n_1 + \frac{n_2}{\tau_{R2}} + \frac{\beta_{51}}{\tau_{R5}} n_5 + \frac{\beta_{41}}{\tau_{R4}} n_4 + \frac{\beta_{31}}{\tau_{R3}} n_3 + K n_2^2 - W_{CR} n_1 n_5 \tag{5}$$

$$\frac{dn_2}{dt} = -\frac{n_2}{\tau_{R2}} + \frac{\beta_{52}}{\tau_{R5}} n_5 + \frac{\beta_{42}}{\tau_{R4}} n_4 + \frac{\beta_{32}}{\tau_{R3}} n_3 + W_{nR}(32) n_3 - 2K n_2^2 + W_{CR} n_1 n_5 + W_{OH}(3) n_3 \tag{6}$$

Table 4
Energy transfers rate parameters (s^{-1}) (expt.).

Er^{3+} (mol.%) density (cm^{-3})	ETU K_0 (s^{-1})	Er^{3+} ($^4I_{11/2}$) → OH^- W_{OH} (3) (s^{-1})	Cross-relaxation W_{CR} (s^{-1})
0.5 (2.3×10^{20})	122	556	4234
1.0 (4.6×10^{20})	5775	948	14,969
2.0 (9.2×10^{20})	9100	1163	44,672
4.0 (1.84×10^{21})	9200	1668	127,650

W_{OH} (2) = 0 (observed in this work).

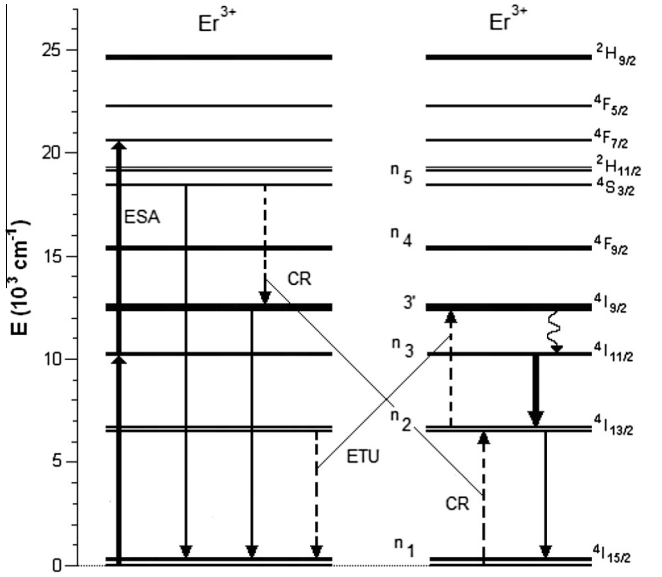

Fig. 8. Energy level scheme and energy transfer mechanism of the Er-doped tellurite glass relevant to the laser operation at 2750 nm. Solid line (up): 976 nm excitation. Solid lines (down): Er^{3+} emissions (552, 813, 1600, and 2750 nm). Dashed lines (up and down): Er^{3+} ETU and CR processes. The energy transfer process to the OH^- radical is not shown.

$$\frac{dn_3}{dt} = R_P n_1 - R_{ESA1} n_3 - \frac{n_3}{\tau_{R3}} - W_{nR}(32) n_3 + \frac{\beta_{53}}{\tau_{R5}} n_5 + \frac{\beta_{43}}{\tau_{R4}} n_4 + W_{nR}(43') n_4 + K n_2^2 + W_{CR} n_1 n_5 - W_{OH}(3) n_3 \tag{7}$$

$$\frac{dn_4}{dt} = -\frac{n_4}{\tau_{R4}} - W_{nR}(43') n_4 + \frac{\beta_{54}}{\tau_{R5}} n_5 + W_{nR}(54) n_5, \tag{8}$$

$$\frac{dn_5}{dt} = R_{ESA1} n_3 - \frac{n_5}{\tau_{R5}} - W_{nR}(54) n_5 - W_{CR} n_1 n_5, \tag{9}$$

where $R_P = \sigma_{13} \frac{I_P}{h\nu_P}$ is the pump rate (s^{-1}), I_P is the pump light (W cm^{-2}), and $h\nu_P$ is the photon energy of pump radiation. β_{ij} represents the luminescence branching ratio and τ_{Ri} is the radiative lifetime of excited states of Er^{3+} labeled as $i = 2$, 3, 4 and 5. The fundamental and excited state absorption cross-sections are $\sigma_{13} = 3.45 \times 10^{-21}$ cm^2 (GSA) and $\sigma_{35} = 1.39 \times 10^{-21}$ cm^2 at 976 nm (ESA). The emission cross-section, $\sigma_{32} = 6.29 \times 10^{-21}$ cm^2 (at $\lambda = 2734$ nm). Experimental values of the intrinsic total decay times (τ_2, τ_3 and τ_5), radiative lifetimes (τ_{Ri}), luminescence branching ratios (β_{ij}), multiphonon decay rates ($W_{nR}(32)$, $W_{nR}(43')$, $W_{nR}(54)$) and W_{OH} (i) ($i = 2, 3$) for the Er^{3+} concentrations used in this work, were given in Table 5.

A quantitative analysis using the numerical solution of the rate equations system of the Er-doped tellurite glasses was carried out in order to characterize the potential for laser emission at ~2.75 μm. The calculated evolution of the excited state populations (in mol.%) obtained by numerical simulation of the rate equations for [Er_2O_3] = 2 mol.% (or 9.2×10^{20} cm^{-3}) using a pumping rate of 2500 s^{-1} (or $I_P = 148$ kW cm^{-2}) is shown in Fig. 9(a), where one can see that equilibrium occurs for a time shorter than 2 ms. At equilibrium, the populations n_3 and n_2 were taken and the population inversion $\Delta n = n_3 - n_2$ was obtained for Er^{3+} = 1, 2 and 4 mol.% as a function of the pump intensity at 976 nm; these results are presented in Fig. 8(b), which indicates a threshold pump intensity that depends on the Er^{3+} concentration (I_P *(threshold)* ~56.5 kW cm^{-2} for the case of [Er_2O_3] = 2 mol.%), where the W_{OH} *(2) = 0 and* W_{OH} (3) = *1163* s^{-1}, i.e., the OH^- effects have been considered in the numerical simulation. This is approximately a factor

Table 5
Parameters used in the rate equation modeling for Er^{3+}-doped tellurite glass.

Transition	β (%)[a]	τ_R[b]	τ (expt.)[c] (W_{nr} (s^{-1}))
Luminescence branching ratio and radiative and intrinsic (total) lifetimes of Er^{3+}[a]			
Er^{3+}:			
$^4S_{3/2}\rightarrow$		374 μs	53 μs (16,348 s^{-1})
$^4F_{9/2}$	0.03		
$^4I_{9/2}$	3.59		
$^4I_{11/2}$	2.21		
$^4I_{13/2}$	27.45		
$^4I_{15/2}$	66.72		
$^4F_{9/2}\rightarrow$		320 μs	23 μs (41,216 s^{-1})
$^4I_{9/2}$	0.29		
$^4I_{11/2}$	1.68		
$^4I_{13/2}$	4.79		
$^4I_{15/2}$	93.24		
$^4I_{9/2}\rightarrow$		2.58 ms	0.83 μs (3.3×10^5 s^{-1})
$^4I_{11/2}$	1.5		
$^4I_{13/2}$	24.8		
$^4I_{15/2}$	73.7		
$^4I_{11/2}\rightarrow$		2.60 ms	314 μs (2801 s^{-1})
$^4I_{13/2}$	15.94		
$^4I_{15/2}$	84.06		
$^4I_{13/2}\rightarrow$		3.27 ms	4.21 ms (~0 s^{-1})
$^4I_{15/2}$	100		
Er_2O_3 (mol.%) (Er^{3+} density (cm^{-3}))	ETU K_0 (s^{-1})	$Er^{3+}(^4I_{11/2})\rightarrow OH^-$ W_{OH} (3) (s^{-1})	Cross-relaxation W_{CR} (s^{-1})
Energy transfer rate parameters (s^{-1}) (expt.)[d]			
0.5% (2.3×10^{20})	122	556	4234
1.0% (4.6×10^{20})	5775	948	14,969
2.0% (9.2×10^{20})	9100	1163	44,672
4.0% (1.84×10^{21})	9200	1668	127,650

[a] Values obtained from the literature for Er^{3+} (<1%)-doped tellurite, [14,15].
[b] Radiative lifetimes calculated using Judd–Offelt theory [6].
[c] Experimental lifetime (intrinsic) obtained from the best fit to the luminescence [6].
[d] Experimental transfer rates obtained in this work.

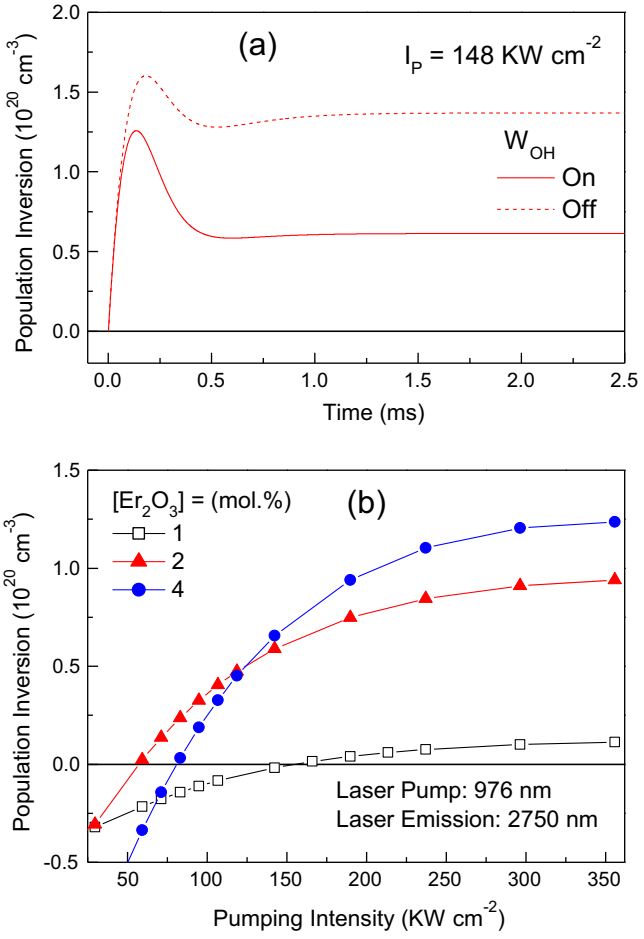

Fig. 9. (a) Calculated population inversion for [Er_2O_3] = 2 mol.% in tellurite glass for CW pumping at 976 nm for varying pumping intensities. W_{OH} (3) was switched off (dashed line) to show its contribution (I_P = 148 kW cm^{-2}). (b) Calculated population inversion as a function of the pump intensity for [Er_2O_3] = 1, 2 and 4 mol.%.

of two lower than our previous study of Er^{3+}-doped tellurite glass whereby water contamination was established to be a problem [6]. In addition, we calculated the population inversion for the $^4I_{11/2}\rightarrow{}^4I_{13/2}$ transition in Er-doped tellurite (2 mol.%) considering W_{OH} (3) = 0 for a CW pump intensity of 148 kW cm^{-2} at 976 nm. The result indicates that the OH effects on the CW laser emission at 2750 nm in the current Er_2O_3 (2 mol.%)-doped tellurite glass reduces by 55% the intrinsic population inversion obtained at the equilibrium (see dashed line in Fig. 9(a)).

One can calculate the population inversion efficiency using the relation $\frac{n_3-n_2}{n}\times100$, where the (n_3-n_2) is the population inversion (given in mol.%) obtained at the equilibrium and n is the total population or the [Er_2O_3] concentration. Fig. 10 shows the calculated population inversion efficiency as a function of the pump intensities for [Er_2O_3] = 1, 2 and 4 mol.%, which shows that the [Er_2O_3] = 2 mol.% gives the most efficient 2750 nm laser emission of tellurite glass for CW pump at 976 nm at T = 300 K.

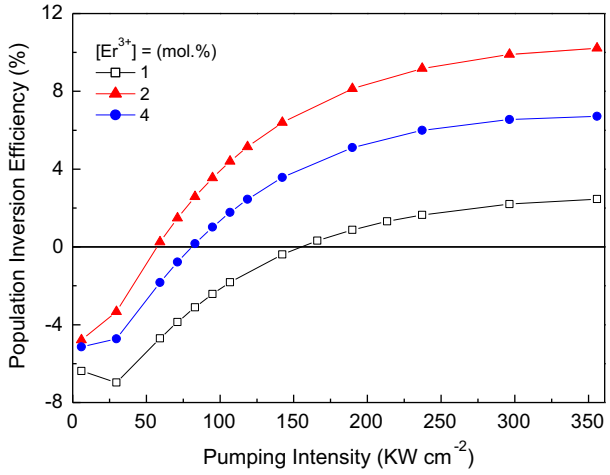

Fig. 10. Calculated population inversion efficiency (%) as a function of the pump intensities for [Er_2O_3] = 1, 2 and 4 mol.% tellurite glass.

5. Conclusions

The intrinsic luminescence efficiency of the $^4I_{11/2}\rightarrow{}^4I_{13/2}$ transition of "water-free" Er^{3+}-doped tellurite glass was determined to be 12%; a value primarily the result of large rates of multiphonon emission. We have observed that only the decay time of the $^4I_{11/2}$ level in our samples was [Er_2O_3] concentration dependent, which we attribute to migration-assisted energy transfer to OH^- radicals present in the glass. The transfer rate from Er^{3+} ($^4I_{11/2}$) to OH^- radicals (at a measured concentration of 2.6×10^{17} cm^{-3}) is ~41% of the multiphonon decay rate for [Er^{3+}] = 9.2×10^{20} cm^{-3} and consequently reduces further the luminescence efficiency to 8.8%. We measured ETU between

excited Er^{3+} ions in the $^4I_{13/2}$ level with a rate increasing with the Er^{3+} concentration; we established that this process is essential for the creation of the population inversion on the laser transition at 2.75 μm, however, the ETU rate constant of 9100 s^{-1} measured for $[Er^{3+}] = 9.2 \times 10^{20}$ cm^{-3} was strong enough to create a population inversion in tellurite glass, even for the possible case where $[OH^-] = 2.6 \times 10^{17}$ cm^{-3}. For $[Er^{3+}] \geqslant 4.6 \times 10^{20}$ cm^{-3} (or Er_2O_3 = 1 mol.%) a population inversion was determined for a threshold pumping intensity of ~154 kW cm^{-2} at 976 nm. It was determined that the Er_2O_3 concentration of 2 mol.% is the best concentration to generate a more efficient population inversion for 2.75 μm laser emission for CW pump at 976 nm, i.e., the population inversion is ~6.8% for I_P = 148 kW cm^{-2}.

Acknowledgments

The authors thank financial support from FAPESP (Grants N^0 1995/4166-0 and 2000/10986-0), CNPq and the Australian Research Council.

References

[1] V. Fortin, M. Bernier, S.T. Bah, R. Vallée, 30 W fluoride glass all-fiber laser at 2.94 μm, Opt. Lett. 40 (12) (2015 Jun 15), http://dx.doi.org/10.1364/OL.40.002882. 2882-5.

[2] T. Hu, S.D. Jackson, D.D. Hudson, Ultrafast pulses from a mid-infrared fiber laser, Opt. Lett. 40 (18) (2015) 4226–4228, http://dx.doi.org/10.1364/OL.40.004226.

[3] S. Duval, M. Bernier, V. Fortin, J. Genest, M. Piché, R. Vallée, Femtosecond fiber lasers reach the mid-infrared, Optica 2 (7) (2015) 623–626, http://dx.doi.org/10.1364/OPTICA.2.000623.

[4] N. Caron, M. Bernier, D. Faucher, R. Vallée, Understanding the fiber tip thermal runaway present in 3 μm fluoride glass fiber lasers, Opt. Express 20 (20) (2012) 22188–22194.

[5] B. Richards, Y. Tsang, D. Binks, J. Lousteau, A. Jha, Efficient ~2 μm Tm^{3+}-doped tellurite fiber laser, Opt. Lett. 33 (4) (2008) 402–404, http://dx.doi.org/10.1364/OL.33.000402.

[6] Laércio Gomes, Michael Oermann, Heike Ebendorff-Heidepriem, David Ottaway, Tanya Monro, André Felipe Henriques Librantz, Stuart D. Jackson, Energy level decay and excited state absorption processes in erbium-doped tellurite glass, J. Appl. Phys. 110 (2011) 083111.

[7] D.L. Rhonehouse, J. Zong, D. Nguyen, R. Thapa, K. Wiersma, C. Smith, A. Chavez-Pirson, Low loss, wide transparency, robust tellurite glass fibers for mid-IR (2–5 μm) applications, Proc. SPIE 8898, Technologies for Optical Countermeasures X and High-Power Lasers 2013: Technology and Systems, 88980D (October 15, 2013).

[8] R. Thapa, D. Rhonehouse, D. Nguyen, K. Wiersma, C. Smith, J. Zong, A. Chavez-Pirson, Mid-IR supercontinuum generation in ultra-low loss, dispersion-zero shifted tellurite glass fiber with extended coverage beyond 4.5 μm, Proc. SPIE 8898, Technologies for Optical Countermeasures X; and High-Power Lasers 2013: Technology and Systems, 889808 (October 15, 2013).

[9] M. Arnaudov, Y. Dimitriev, V. Dimitrov, M. Dimitrova-Pankova, Infrared spectral investigation of water in tellurite glasses, Phys. Chem. Glasses 27 (1986) 48.

[10] H. Gebavi, D. Milanese, G. Liao, Q. Chen, M. Ferraris, M. Ivanda, O. Gamulin, S. Taccheo, Spectroscopic investigation and optical characterization of novel highly thulium doped tellurite glasses, J. Non-Cryst. Solids 355 (2009) 548–555.

[11] L. Nemec, J. Gotz, Infrared Absorption of OH- in E Glass, J. Am. Ceram. Soc. 53 (1970) 526.

[12] A.I. Burshtein, Hopping mechanism of energy transfer, Sov. Phys. JETP 35 (1972) 882–885.

[13] L. Gomes, A.F.H. Librantz, F.H. Jagosich, W.A.L. Alves, I.M. Ranieri, S.L. Baldochi, Energy transfer rates and population inversion of $^4I_{11/2}$ excited state of Er^{3+} investigated by means of numerical solutions of the rate equations system in Er: $LiYF_4$ crystal, J. Appl. Phys. 106 (2009) 103508.

[14] C. Li, Y. Guyot, C. Linares, R. Moncorgé, M.F. Joubert, Radiative Transition Probabilities of Trivalent Rare-Earth Ions in LiYF4, in: Proceedings on Advanced Solid-State Lasers, Albert A. Pinto, Tso Yee Fan, Vol. V of OSA Proceedings Series (Optical Society of America, New Orleans, LA., 1993), pp. 91–95.

[15] Y. Zhanci, H. Shihua, L. Shaozhe, C. Baojiu, Radiative transition quantum efficiency of $^2H_{11/2}$ and $^4S_{3/2}$ states of trivalent erbium ion in oxyfluoride tellurite glass, J. Non-Cryst. Solids 343 (2004) 154.